

RECEIVED JUN 29 200

AFRL-SR-AR-TR-05-

0307

REPORT DOCUMENTATION PAGE

Public reporting burden for this collection of information is estimated to average 1 hour per response, including the time for reviewing instructions, searching existing data sources, gathering the required data, and completing and reviewing this collection of information. Send comments regarding this burden estimate or any other aspect of this collection of information, including suggestions for reducing this burden to Washington Headquarters Services, Directorate for Information Operations and Reports (0704-0188), 1215 Jefferson Davis Boulevard, Arlington, VA 22202-4302. Respondents should be aware that notwithstanding any other provision of law, no person shall be subject to any penalty for failing to comply with a collection of information if it does not display a unique OMB control number. PLEASE DO NOT RETURN YOUR FORM TO THE ABOVE ADDRESS.

1. REPORT DATE (DD-MM-YYYY) 14-06-2005		2. REPORT TYPE Annual Technical Report		3. DATES COVERED (From - To) From 2/2004 to 2/2005	
4. TITLE AND SUBTITLE (THEME 3) Meso and Micro Scale Propulsion Concepts for Small Spacecraft				5a. CONTRACT NUMBER	
				5b. GRANT NUMBER FA9550-04-1-0088	
				5c. PROGRAM ELEMENT NUMBER	
6. AUTHOR(S) R.A. Yetter [†] , V. Yang [†] , I. A. Aksay [†] and F.L. Dryer [*]				5d. PROJECT NUMBER	
				5e. TASK NUMBER	
				5f. WORK UNIT NUMBER	
7. PERFORMING ORGANIZATION NAME(S) AND ADDRESS(ES) [†] Department of Mechanical and Nuclear Engineering The Pennsylvania State University University Park, PA 16802 [*] Department of Chemical Eng. and Aerospace Engineering Princeton University Princeton, NJ 08544				8. PERFORMING ORGANIZATION REPORT NUMBER	
9. SPONSORING / MONITORING AGENCY NAME(S) AND ADDRESS(ES) AFOSR ATTN: Dr. Mitat Birkan 801 North Randolph Street Room 732 Arlington, VA 22203-1977 NA				10. SPONSOR/MONITOR'S ACRONYM(S)	
				11. SPONSOR/MONITOR'S REPORT NUMBER(S)	
12. DISTRIBUTION / AVAILABILITY STATEMENT Unlimited Distribution					
13. SUPPLEMENTARY NOTES					
14. ABSTRACT A meso/micro scale liquid propellant thruster is being developed for small spacecraft. In this thruster, the liquid propellant was injected directly into the chamber tangentially along the combustor wall. Heat feedback from the flame, once ignited, decomposed and gasified the liquid propellant. The gasification process of the propellant produced a vortex flow in the combustor, which stabilized the gas-phase flame. Modeling studies with gas-phase injection of reactants have shown that the vortex flow creates various flow recirculation patterns depending upon the Reynolds numbers of the flows. Although the propellant of interest was a HAN based liquid propellant, initial studies were conducted with liquid nitromethane. Operation of the combustion chamber with pure nitromethane at chamber pressures as high as 30 atm was studied. To gasify and initially ignite a HAN based propellant, techniques that make use of the electrolytic character of the propellant were investigated. In particular, a continuous flow igniter with titanium electrodes and a gap spacing of 500 μm was developed and studied. Results showed that a small voltage drop across the electrodes ignites the continuous flow, which can then be removed to achieve a steady-state decomposition process. Methods to further miniature, fabricate, and package the entire system will be investigated in the future.					
15. SUBJECT TERMS Meso and Micro Scale Combustion and Propulsion, Electrolytic Ignition, Ceramic Stereolithography					
16. SECURITY CLASSIFICATION OF: Unclassified			17. LIMITATION OF ABSTRACT	18. NUMBER OF PAGES 26	19a. NAME OF RESPONSIBLE PERSON Richard A. Yetter
a. REPORT	b. ABSTRACT	c. THIS PAGE			19b. TELEPHONE NUMBER (include area code) (814) 863-6375

7-25-05

TABLE OF CONTENTS

Abstract	1
Table of Contents	2
Introduction	3
Brief Summary of Previous Research on Gas-Phase Mixtures	4
Research Progress	10
Liquid Propellant Combustion	10
Electrolytic Ignition	15
Model Development and Analysis of Vortex Flows	19
Summary	23
Publications and Presentations	24
References	25

INTRODUCTION

Two developing technology areas in the field of microelectromechanical systems (MEMS) are micropower generation and micropropulsion [1-5]. Combustion research is expected to play an important role towards the success of both these areas, which have recently been reviewed in the literature [6,7]. Microthrusters, because of their simplicity, have received significant attention during the last few years, although early development in the MEMS field began approximately 10 years ago [8-16]. The principle applications of microthrusters are for primary propulsion and attitude control of microspacecraft, but they may also be applied to any process requiring small quantities of directed gas flows. For example, the same technology necessary for the successful development of micro-thrusters is currently being applied to micro gas generators for usage in airbags and in microactuators [17-19].

As a recent example of the development of micro-spacecraft and the need for micro-thrusters, the US Air Force's XSS-10 microsatellite experiment flew on 29 January 2003 as a secondary payload to a Global Positioning System navigation satellite aboard a Delta 2 rocket [20]. The micro-satellite weighed 28 kilograms and represented the first work in space involving micro-satellites that can autonomously approach other objects in space. The experiment was also the first in which the Air Force activated the satellite hours after the launch versus a normal on-orbit checkout ranging from weeks to months. Shortly after reaching space, the XSS-10 spacecraft maneuvered about 200 meters away from the rocket, and then approached it, taking video imagery that was transmitted live to the ground. The experiment also provided information that researchers are now incorporating into follow on missions called XSS-11, which is a yearlong test of microsatellite technologies. More importantly, the XSS-10 experiment represented a significant step in transforming the way the Air Force can operate in space.

For solid propellant rockets, the interest in microthrusters results from the potential gain in thrust-to-weight ratio (F/W) with downsizing. Thrust is proportional to the characteristic length squared, $F \propto P_c A_t \propto \ell^2$, where P_c is the combustion chamber pressure and A_t is the nozzle throat cross-sectional area. Because initial weight of a solid propellant thruster is approximately proportional to volume (ℓ^3), the thrust-to-weight ratio is inversely proportional to length scale ($F/W \propto \ell^{-1}$). Thus, if a one-meter macro-scale thruster has a thrust-to-weight ratio of 10, a thruster with a length scale of 1 cm could potentially have a thrust-to-weight ratio of 1000 and a thruster with a length scale of 1 mm could have a thrust-to-weight ratio of 10,000. If achievable, the applications of microthrusters could be numerous, ranging from distributed propulsion in macro-scale systems to primary propulsion in micro-scale systems. Although potential gains are

also expected with scaling of liquid and gas thrusters, such scaling is not as simplistic as with solid propellant thrusters and therefore may not directly apply. The actual gains and optimal microthruster designs will require multidisciplinary research efforts of experimentation, advanced diagnostics, modeling analysis and materials fabrication.

This annual report describes the progress made over the last year on an AFOSR project to develop and analyze a liquid monopropellant microthruster. Previously, we investigated the following aspects towards the development of this microthruster: (1) combustion of gaseous hydrocarbon fuels and air or oxygen enriched air in small volumes using vortex flows to improve combustion stability and minimize heat losses, (2) electrolytic gasification and decomposition of liquid propellants as a means for ignition while minimizing power requirements and system complexity, (3) fabrication of axisymmetric ceramic thrusters for high temperature operation and materials compatibility with propellants and silicon based control modules, (4) testing and diagnostics of the ceramic thrusters, and (5) numerical model development for analysis and engineering design of the combustion chambers and thrusters.

The emphasis of last year's research was on (a) experiments that would demonstrate the ability to operate the thruster on liquid monopropellants, (b) the development and analysis of a small scale continuous flow electrolytic igniter system, which could be adapted to the vortex combustor, (c) numerical analysis of the flame dynamics and flame stabilization processes in the combustor when fueled with gaseous reactants, and (d) numerical model development for describing liquid propellant injection and subsequent gasification in the combustor. In order to compare liquid propellant operation of the combustor with the gaseous reactant operation, a brief summary of the prior results [21] is provided before discussing last year's progress.

BRIEF SUMMARY OF PREVIOUS RESEARCH ON GAS-PHASE MIXTURES

As combustion volumes are reduced in size, issues of residence time (finite-rate chemistry), fluid mixing (laminar flows, small length scales), heat loss management (high surface to volume ratios), and wall quenching of gas-phase reactions become increasingly more important. In the present program, many of these issues are addressed by application of the asymmetric whirl combustion concept [22] in which fuel is injected off axis of a rotating air flow. The concept of the asymmetric whirl combustor is shown in **Fig. 1** for stabilization of a gaseous fuel-air mixture. Air flow enters the combustor tangentially without an axial component. The axial component is determined by mass conservation in which fresh mixture displaces the reacting mixture forcing it

down the combustor axis. The air continues its rotating flow pattern by exiting tangentially or axially at the opposite end of the combustor.

An example of the combustor operating on a propane / air mixture with an overall equivalence ratio of 0.8 is given in **Fig. 2**. The flame appears as a luminous blue ring with a non-

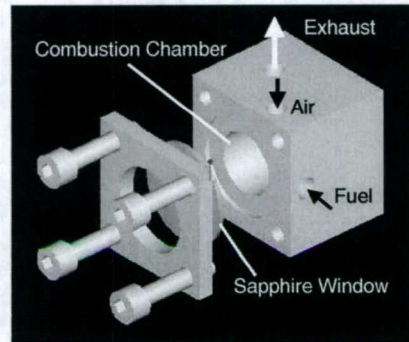


Figure 1. Meso-scale whirl combustor showing reactant inlet ports, exhaust port, combustor chamber and observational window.

luminous core. The quench layer is again approximately 0.5 mm thick. This combustor had an internal diameter of 6 mm and a length of 6 mm. The overall combustor volume was approximately 170 mm^3 . For this combustor size, the inner diameter of the fuel jet tube was $500 \mu\text{m}$, while the inner diameter of the air jet tube was $760 \mu\text{m}$.

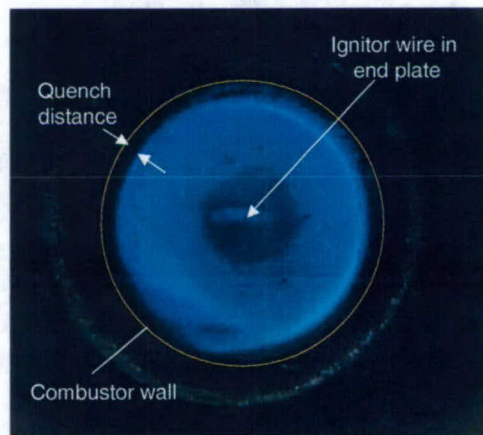


Figure 2. Meso-scale whirl combustion of propane air with an equivalence ratio of 0.8. The swirl number was 70. The Re number of the inlet air jet was 1780 and the Re number of the propane inlet jet was 310. The theoretical chemical input power was 50 W.

The ring flame structure results from fuel injection into the region of highest kinetic energy of the whirling air flow, thereby producing rapid fuel-air mixing. The resulting flow produces a central hot combustion product core and a surrounding spinning outer flame zone with extremely

good flame stability at low overall equivalence ratios. Experiments have shown that the combustor exhibits an unusual wide range of stability margin, even for overall equivalence ratios below $\phi = 0.1$. The combination of tangential injection of air and tangential exit of combustion products appears to create a low-pressure trough along the centerline of the combustor. The Rayleigh criterion predicts that hot, low-density combustion product gases are trapped in this trough. This hot central core stabilizes the flame by acting as a source of enthalpy and radicals. Furthermore, the rotating flow internally re-circulates a portion of the hot combustion products into the fresh unreacted mixture entering the combustor, producing somewhat of a stirred reactor concept. The introduction of cold reactants about the circumference and the formation of the radial pressure gradient also enable the combustor walls to remain cooler than the hot central core.

A set of combustors, designed by scaling the Damköhler and Reynolds numbers and ranging in volume from 10 to 108 mm³ and fabricated using EDM, is shown in **Fig. 3**. In experiments conducted to evaluate the flame stability and performance characteristics, fuel and air flow measurements were made with Hastings mass flow meters, which have been cross calibrated with results obtained from bubble meter measurements. The fuels tested were hydrogen (99.9 % purity), methane (99.5 % purity), and propane (98 % purity). Ignition was achieved by hot wire ignition using a 250 μ m diameter nichrome wire mounted on the end plate at the center of the combustor and also by spark discharge at the same location.

Lean and rich blow-off limits were obtained by fixing the air flow rate, igniting the combustor at a stable condition (typically at an overall equivalence ratio near 0.8) and then either

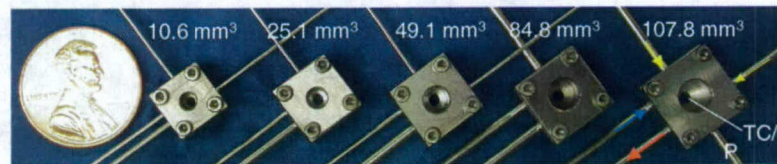


Figure 3. Meso-scale combustors for combustion scaling analysis. The hole at the back end of the combustion chamber is for igniter insertion.

decreasing or increasing the fuel flow rate until the reaction extinguished at which point the fuel flow rates were recorded to determine the lean and rich limits, respectively. In the present context, equivalence ratio is defined for the entire combustion chamber volume. Since the fuel and oxidizer are injected separately into the chamber, the local equivalence ratio can vary from zero to infinity in the chamber.

In all of the meso-scale combustors, stable operation was achieved with H₂ / air mixtures for overall equivalence ratios ranging from approximately 0.3 to 6. **Figure 4** reports stability limits as a function of total flow rate for the 49 mm³ combustor and temperature as a function of overall equivalence ratio. For methane and propane, stable hydrocarbon combustion was attained with air at atmospheric pressure in the three largest combustors. For the smallest combustors, air enriched with small quantities of oxygen was required to achieve stable combustion at atmospheric pressure.

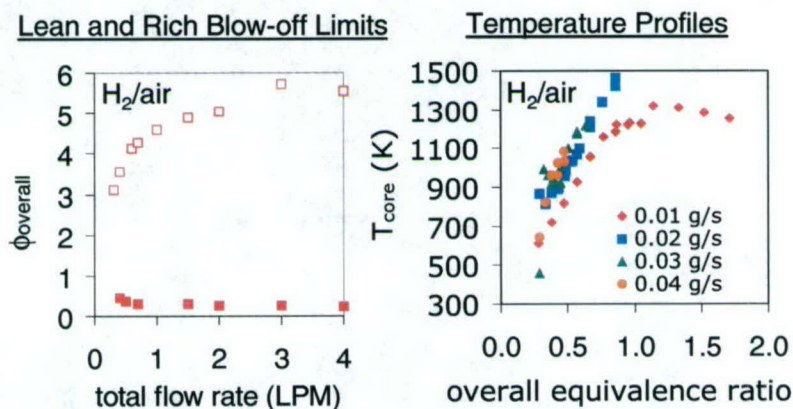


Figure 4. (a) Stability limits for hydrogen air combustion in the 49 mm³ meso-scale combustor. (b) Temperature measurements for hydrogen air combustion inside the 49 mm³ meso-scale combustor on the combustor centerline near the lean flammability limit.

Figure 5a gives the lean and rich blow-off limits as a function of air flow rate for propane as the fuel. Blow-off limits appear to increase with increasing airflow rate. Over the range of air flow rates investigated, the separation in equivalence ratio remains nearly constant. For propane, air flow rates were varied from 700 to 1250 cm³/min. At 700 cm³/min, the lean and rich blow-off limits were measured to occur at overall equivalence ratios of approximately 0.2 and 1.3, respectively. With an air flow of 1250 mm³/min, the lean and rich blow-off limits occurred at overall equivalence ratios of approximately 0.4 and 1.6, respectively. The lean and rich flammability limits, based on equivalence ratio, of propane in air are 0.56 and 2.7, respectively. Operation of the combustor on mixtures leaner than the lean flammability of a premixed mixture suggests that some stratification remains in the mixture during combustion. For fuel-lean mixtures, the flame appeared as a blue luminous ring. For fuel-rich mixtures, the flame was bluish-green. Under no conditions did the flame have a yellow emission characteristic of soot formation. Carbon deposits have also not been observed on any of the surfaces.

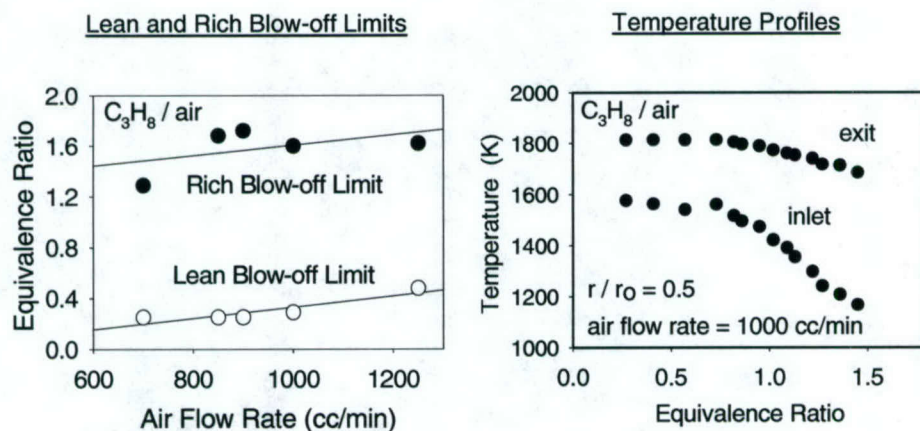


Figure 5. (a) Stability limits for propane air combustion in the 170 mm³ meso-scale combustor. (b) Temperature measurements for propane air combustion inside the 170 mm³ meso-scale combustor with an air flow rate of 1000 cm³/min at a radial position of $r/r_o = 0.5$ for two different axial positions.

Temperature measurements as a function of equivalence ratio for propane as the fuel at an air flow rate of 1000 cm³/min are presented in **Fig. 5b**. The measurements were obtained with a 76 μ m diameter bare wire Pt/Pt-13%Rh thermocouple located at a radial position of half the radius at two axial locations, one near the reactant entrance and the other near the product exit. The measurements have not been corrected for radiation or conductive losses and coatings to prevent catalytic surface reactions have not been used. The adiabatic flame temperature for a propane air mixture with an overall equivalence ratio of 0.75 is approximately 1970 K. The inferred differences between measured and theoretical temperatures likely result from the heat losses of the meso-scale device, but could also result from incomplete combustion and uncertainties in the temperature measurements themselves.

Examples of the chemical efficiency of the combustion process for the smallest combustion chamber volumes at a fixed residence time as a function of overall equivalence ratio are shown in **Fig. 6** for hydrogen-air combustion and methane with oxygen enriched air. In the case of hydrogen combustion, the chemical efficiency was determined by measuring the exhaust gas composition and considering what fraction of the original H₂ was converted to H₂O. These measurements were obtained by sampling the entire exhaust with an Aligent 3000A micro gas chromatograph (hydrogen, oxygen, and water vapor) and a Nicolet Nexus 670 Fourier Transform Infrared (FTIR) spectrometer (water vapor). Sample lines were heated and the composition measured without drying the sample. For hydrogen combustion, scaling effects were essentially not observed in the combustion process. Above an overall equivalence ratio of approximately 0.4, all combustors were extremely stable with chemical efficiencies approaching 100%. Based upon exhaust gas temperature measurements and comparison of these temperatures with the theoretical

equilibrium value, thermal efficiencies were considerably lower, ranging from approximately 60 to 80%. No attempt was made to insulate the combustors.

Figure 6 also shows the chemical efficiency of the 10 and 49 mm³ combustors operating on an oxidizer mixture consisting of 40% oxygen and 60% nitrogen as a function of overall equivalence ratio for a fixed residence time. The chemical efficiency was determined from

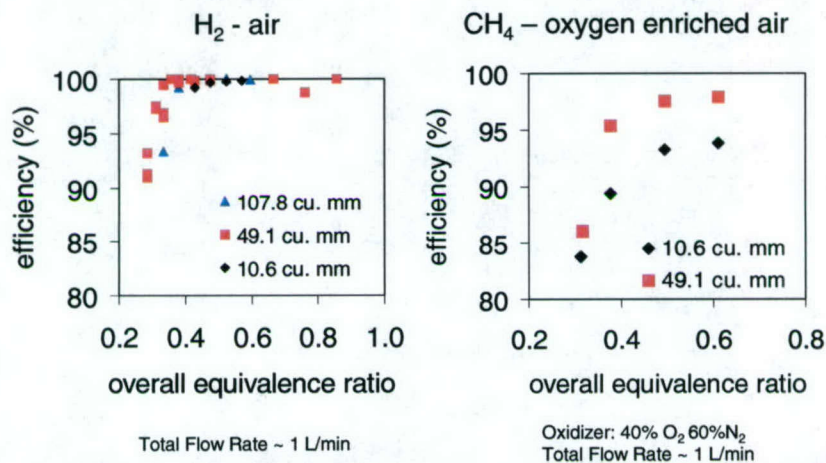


Figure 6. Chemical efficiency of hydrogen air combustion and methane oxygen enriched air combustion in different size combustors as a function of overall equivalence ratio.

exhaust gas composition measurements using FTIR spectroscopy. The species concentrations measured included CO, CO₂, CH₄, C₂H₂, C₂H₄, and C₂H₆ and chemical efficiency was determined by evaluating the fraction of carbon in the fuel that was converted to CO₂. Stable operation was achieved with overall equivalence ratios as low as 0.2. For overall equivalence ratios above 0.4, scaling effects were observed between the different combustors. In the present case, the 10 mm³ combustor had chemical efficiencies near 93% whereas the 49 mm³ combustor had chemical efficiencies near 98%. Further oxygen enrichment also showed a clear change in the flame structure and for the limiting case of pure oxygen, the flame appeared more as a micro diffusion flame stabilized at the tip of the fuel entrance jet. The change in flame structure resulted from the mixing time exceeding the chemical time. The pure oxygen flame burns at a higher flame temperature and therefore the kinetics are considerably faster. In addition, for pure oxygen operation, the flow was achieved by simply eliminating the nitrogen in the oxidizer inlet flow. Therefore, the oxidizer jet momentum was reduced, which also increased the mixing time.

RESEARCH PROGRESS

Liquid Propellant Combustion

The previous results were encouraging, particularly since air will not be the oxidizer used in the thruster. The actual thrusters are intended to operate on liquid homogeneous monopropellants. The advantages of monopropellants are the simplicity of the resulting system design, reduction in hardware, and the ability of selecting the physical and performance properties of the propellant to fit the particular application. The propellant formulations include an energetic oxidizer, an alcohol fuel, and water as the liquid carrier. Hydroxylammonium nitrate (HAN, $\text{NH}_3\text{OH}^+\text{NO}_3^-$), hydrazinium nitroformate (HNF, $\text{N}_2\text{H}_5^+\text{C}(\text{NO}_2)_3^-$), and ammonium dinitramide (ADN, $\text{NH}_4^+\text{N}(\text{NO}_2)_2^-$) are solids with ionic structures that are water-soluble and serve as the primary propellant oxidizers. Other hydrocarbons, such as alcohols, which are also soluble in water, serve as the fuels. These types of formulations have been proposed and studied by others [23-26]. Considering the ingredients and products of combustion, the propellant formulations are expected to have good physical and environmentally friendly property characteristics for micro-spacecraft propulsion applications. The low to moderate flame temperature of these propellant formulations is an additional attractive feature for microscale applications. For nearly equivalent Isp levels as hydrazine, the resulting propellant densities are generally higher.

Using the same concept to achieve stable combustion as with the gaseous reactants, experiments were performed with liquid propellants in which vortex flows were obtained by injecting the liquid propellant tangentially along the combustor wall (Fig. 7) just as the bulk air flow was in the gaseous reactant systems. However, in this configuration, the liquid flow can

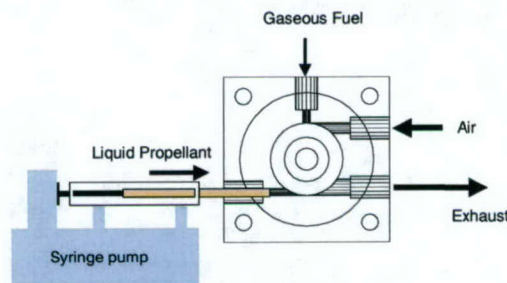


Figure 7. Schematic of tangential injection of liquid monopropellant into vortex combustion chamber.

form a film along the surface of the combustor walls. In the present research, the film may be used to cool the walls because of both endothermic liquid decomposition reactions and gasification, which can produce improved thermal management at the small scales of the present systems. Because the liquid is a monopropellant, once gasified, the reactants do not need to be

mixed as in the previous research with gaseous reactants. For steady-state operation, the hot chamber walls and heat feedback from the gas-phase was used to continuously gasify the

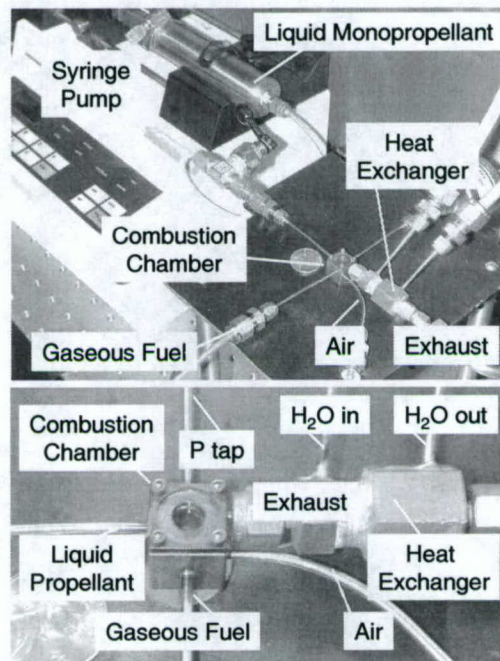


Figure 8. Experimental setup for liquid monopropellant injection initiated by gaseous fuel / air combustion.

propellant. The present research thus differs from that of Stanchi et al. [27] where tangential film injection of liquid hydrocarbon fuels in small combustors with axial air flow is under study.

Figure 8 is a photograph of the experimental setup illustrating the combustion chamber, the inlet and outlet, the exhaust heat exchanger, and the fuel syringe pump. To demonstrate the capability to operate on liquid fuels, studies were initiated with liquid nitromethane, since it is a simple liquid monopropellant and its ignition and combustion behavior are relatively well understood. In future studies, the nitromethane will be replaced with a HAN based formulation. In these experiments, the 108 mm^3 combustor was initially ignited on a methane / oxygen mixture with an equivalence ratio of approximately 0.5. Liquid nitromethane was then injected tangentially through another inlet port at the entrance of the combustion chamber as shown in **Figs. 7** and **8**. Once the nitromethane flame was established, the methane gas flow was shut-off and the oxygen flow rate was decreased. For experiments operating at one atmosphere, it was found that the oxygen flow could not be completely shut off and still maintain combustion. The lowest oxygen concentration for which a stable nitromethane flame was achieved was 6 % by volume. The resulting flame is shown in **Fig. 9** and produces a yellowish, bright-white emission. As in the combustion of the gaseous hydrocarbon / air mixtures, no soot or carbon deposits were

observed to form on the surfaces. Thermodynamically, if the oxygen is eliminated from the mixture with 94% nitromethane, predicted flame temperatures decrease about 100 K.

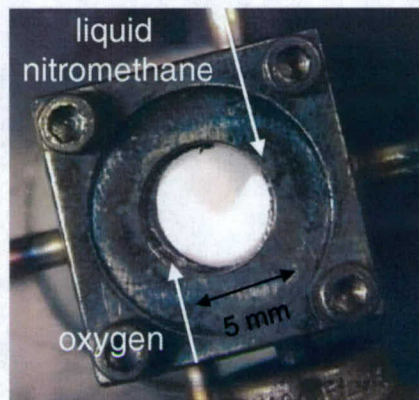


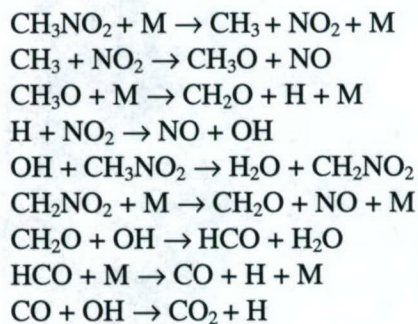
Figure 9. Combustion of 94% by volume liquid nitromethane / 6% by volume oxygen mixture. The emission of the nitromethane flame is a brownish bright white color as compared to the bright blue emission observed from the gaseous hydrocarbons. No carbon deposits or soot formation is observed in either case. The theoretical chemical input power was 97 W. The volume of the combustion chamber was 108 mm³ and the chemical power input was 160 W.

A detailed reaction mechanism for the thermal decomposition of gaseous nitromethane was developed and used to investigate the effects of oxygen addition on the rate of decomposition. This mechanism was developed by comparison of model predictions with experimental data obtained from shock tube and static reactor experiments. The data encompassed a combined temperature range of 700-1494K and pressure between 0.1 and 5.73 atmospheres. **Table 1** shows an example of the comparisons between model prediction and literature experimental data for induction times as a function of temperature and pressure.

Table 1. Comparison of Calculated and Experimental Induction Times

%CH ₃ NO ₂	P(atm)	T(K)	$\tau_c(\mu s)$	$\tau_e(\mu s)$
49	2.18	1440	2.5	4
100	5.73	1494	0.5	<1
100	6.17	1376	1.5	2-3
100	4.82	1227	10	10-12
100	3.76	1155	35	25-30
100	4.0	1120	60	35

Nitromethane, CH₃NO₂, is a monopropellant that is relatively unreactive at one atmosphere in an inert environment. The need for the small amount of oxygen at one atmosphere can be understood by looking at its combustion kinetics relative to that of a hydrocarbon-oxygen system. The most important steps to nitromethane combustion are as follows:



Unlike hydrocarbon oxidation which has significant chain branching due to the presence of molecular oxygen (via. $\text{H} + \text{O}_2 \rightarrow \text{OH} + \text{O}$), no equivalent branching reactions occur in the nitromethane system. The main source of radicals is through pressure dependent dissociation reactions. Consequently, at low pressures, nitromethane kinetics are slow, but accelerate dramatically with pressure. Because of chain branching in hydrocarbon systems, reaction rates at low pressure can be fast and do not increase as much with pressure as in the case of nitromethane.

In the atmospheric pressure experiments, the little amount of oxygen added to the system provides the initiation chain branching necessary at low pressure to achieve stable combustion. This added oxygen can be eliminated from the system by simply operating at higher pressures.

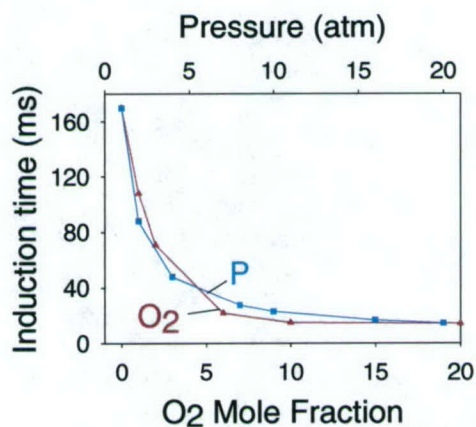


Figure 10. Homogeneous ignition of gaseous nitromethane as a function of pressure and oxygen perturbation.

The effect of an increased pressure on nitromethane kinetics is shown in **Fig. 10**. In this figure, homogeneous gas-phase kinetics calculations were performed using the detailed reaction mechanism for nitromethane decomposition kinetics. The O_2 line shows the induction time of a mixture with initially 100% nitromethane and the effect of adding a small amount of oxygen to the mixture. Induction time is used here mainly as an indication of reaction rate, i.e., the shorter

the induction time the faster the chemistry. In the atmospheric pressure experiments, 6% oxygen was required to stabilize a flame. According to **Fig. 10**, this represents about a factor of 5 acceleration in the kinetics, relative to the mixture without oxygen. The pressure (P) line in the figure shows the effect of pressure on induction time of pure nitromethane. As with increasing oxygen, an increase in pressure also accelerates the kinetics. This figure suggests that a pressure of at least 7 atm would be required to stabilize the flame in the combustor (i.e., to achieve approximately the same induction time when 6% oxygen was added to nitromethane at atmospheric pressure).

In order to operate the combustion chamber at elevated pressures, the saffire observation window (0.5mm thick) needed to be replaced. This window was replaced with a solid inconel end cap that had a thermocouple, which protruded slightly into the combustion chamber. The thermocouple had a metal sheath, and thus experienced significant heat lost relative to the true gas phase temperature.

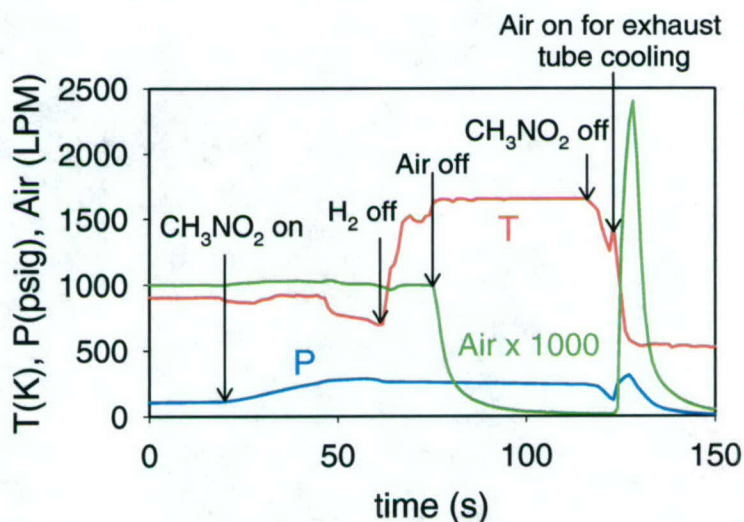


Figure 11. Steady-state operation of the 108 mm³ combustor on liquid nitromethane at 8 atm.

Figure 11 shows the successful operation of the combustor on 100% liquid nitromethane at a pressure of 8 atm. In the figure, the combustion process was initiated with a very lean hydrogen air mixture (temperature approximately 900K). As liquid nitromethane was added to the combustor, the hydrogen was first turned off and then the air was turned off. Stable combustion continued on pure liquid nitromethane. The experiments have been repeated at pressures above eight atmospheres and stable combustion has been achieved. The 0.5 mm thick saffire window was subsequently replaced with a 2 mm thick window and **Fig. 12** shows the combustion process at a pressure of approximately 23 atm. Combustion occurs within the

chamber, but because of the thin walls of the exhaust tube, its temperature achieves extremely high values. The chamber is also partially cooled by the liquid film injection along the walls.

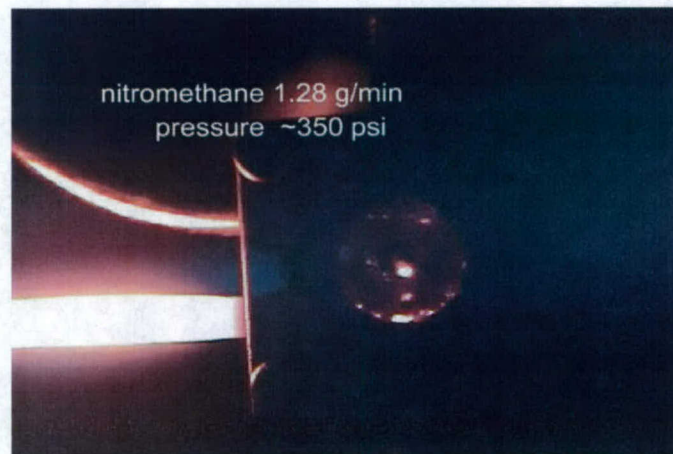


Figure 12. Steady state combustion of pure liquid nitromethane in the 108 mm³ combustor operating at approximately 23 atm.

Inside the chamber, small specks of bright luminosity are observed. These bright spots are suspected to be carbon deposits or soot formation. However, after combustion, the internal walls are not covered with any deposits.

Electrolytic Ignition

As mentioned above, HAN-based propellants are of interest for several reasons. They are environmentally “green”, have good energy densities, and offer a unique means for ignition in small-scale devices. In aqueous solutions, as the concentration of HAN is increased in the formulations, ion-pairs are formed [28] and the liquid becomes electrolytic. Proton transfer between the ion pairs generally initiates thermal decomposition. When the initial concentrations exceed 2M, the HAN molecule begins to form the ion-pair that connects the OH group hydrogen of NH_3OH^+ to the oxygen of NO_3^- . This ion pair becomes the dominant species in solution with concentrations greater than 11M. Along with the ion pair, hydrogen bonding can be formed between the OH group of HAN and the solvent water, causing a high solubility of the salt mixtures.

We have shown in our previous research that because the liquids are electrolytic, electrolysis may be used for primary ignition or for ignition assistance. Here, energy is deposited directly into the liquid and not the surroundings (as in thermal heating) causing non-spontaneous redox reactions to occur. These reactions may alter the rate controlling steps of the thermal decomposition mechanism, thereby lowering the effective activation energy and the initiation

temperature for decomposition / gasification. Furthermore, new exothermic reactions may be initiated further reducing the external energy requirement.

In our previous effort, we examined the electrolytic ignition characteristics of HAN-based liquid propellants. The experiments involved filament suspended micron-sized droplets. The propellants considered were XM46, a HAN methanol mixture consisting of hydroxylammonium nitrate (HAN, 69.7 wt%), methanol (CH_3OH , 14.79 wt%), water (H_2O , 14.91 wt%), and ammonium nitrate (AN, 0.6 wt%), and RK315A, another HAN based mixture of interest to the Air Force. Voltage drops across two small electrodes inserted into the droplet were measured along with the resulting liquid resistance and power requirements necessary to achieve gasification and ignition. The droplet was suspended by a bead at the end of a quartz fiber. Two

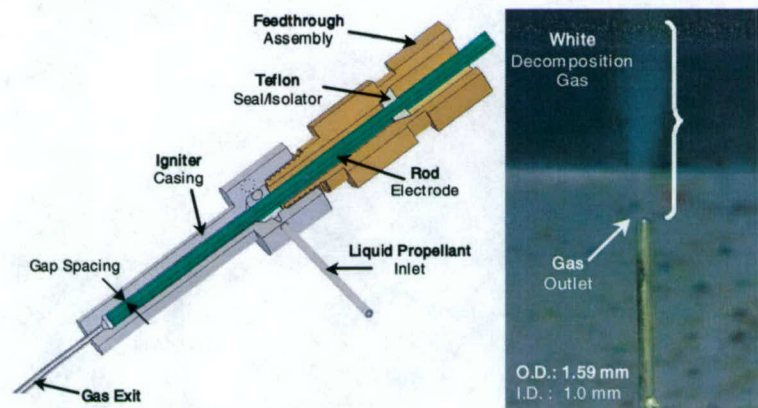
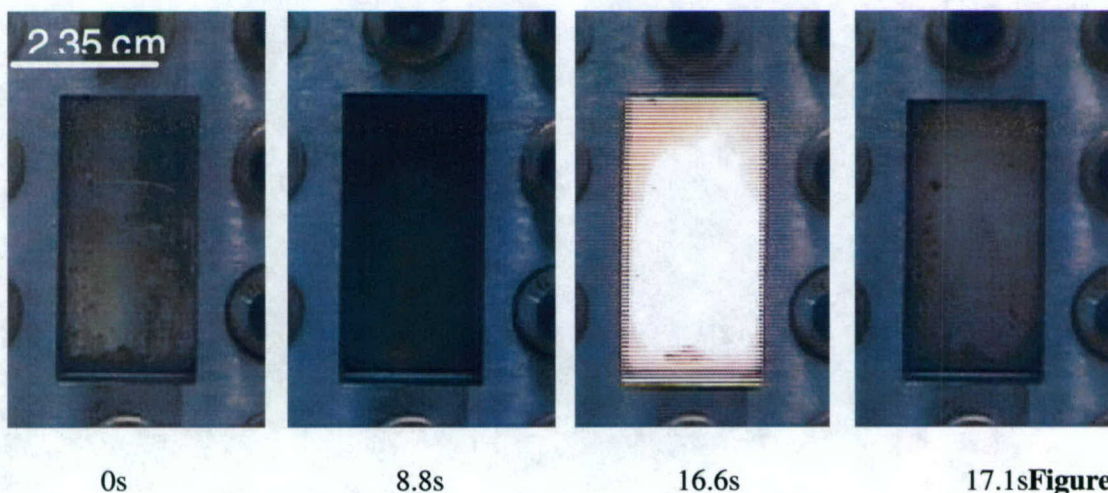


Figure 13. Meso-scale igniter system with 500 μm electrolysis channels.

nichrome (80%Ni/20%Cr) or platinum wires, with diameters of 250 μm acting as electrodes, were inserted into the liquid propellant droplet. The gap between the two electrodes was varied, but was nominally of the order 1mm. During an experiment, a Hamilton syringe was used to suspend the droplet to the bead of the fiber. The electrodes were then moved to the center of the droplet. A DC power supply was used to supply a controllable voltage drop ranging from 0 to 15V across the electrodes. By connecting the electrodes in a series circuit to a resistor, and then measuring the voltage across the resistor, the current through the droplet was determined. These voltages, including the voltages across the resistor and across the droplet were recorded by a National Instruments data acquisition system. Results from these experiments indicated that both gasification and ignition was observed.

During the past year, we have been studying electrolysis in continuous flow igniters at scales that can be integrated with the meso/micro scale thrusters. An example of an igniter is shown in **Fig. 13**. The igniter employs a titanium electrode cathode rod encased in a small titanium chamber that serves as the anode. For the rod igniter, the total electrode surface area is 1200 mm^2 with a $500 \text{ }\mu\text{m}$ gap between the anode casing and the cathode rod. The inlet and exit ports have an outer diameter of 1.6 mm and an inner diameter of 1.0 mm . The liquid propellant enters into the anode casing and then flows through the annular region of the igniter where the voltage potential was applied. While flowing through the gap, the liquid propellant gasifies and exits the



14. Images of gas above fin electrodes during and after ignition

igniter assembly. **Figure 13** also shows a captured image of the decomposition products of RK315A exiting out of the miniature rod igniter. The flow rate of the propellant was 0.35 in/min resulting in a mass flow rate of 0.0115 g/s entering the igniter and the voltage potential was set at 26 VDC . In the figure, white smoke was observed above the gas outlet, which is indicative of low-pressure decomposition products of RK315A. Subsequent to observing a continuous white stream of smoke exiting the igniter, the voltage input source was removed, thereby allowing the incoming propellant to continue to self-decompose without a voltage driving potential. A thermocouple was placed in the middle of the igniter on the outer surface of the anode casing. The wall temperature reached a maximum of 120°C and continued to maintain a steady temperature during the test run. This value indicates that the casing was maintained at the decomposition temperature of RK315A and verified that liquid was present in the igniter assembly. These results are very encouraging; particularly since no optimization of material or igniter design was performed.

The continuous flow igniter has now been connected to the combustor and testing on the coupled igniter-combustor system will be performed during the near term. Methods to further miniature, fabricate and package the entire system will be investigated in the future. The igniter design shown in **Fig. 13** may also be usable by itself as a warm gas thruster operating on the same propellant as the hot gas thruster currently under development.

To understand more about how the continuous flow igniter functioned, experiments are also shown here from a larger scale system in which a series of electrode fins were used as the electrolysis cell [29]. Liquid was passed through the fins with a voltage potential applied and the gas generated at the exit of the fins was observed with the pressure and temperature in the igniter chamber. The chamber pressure was regulated by using an interchangeable graphite nozzle with a specified throat diameter of 1.5 mm (0.059 in) at the exit of the chamber above the electrodes. The instantaneous pressure was recorded using a Setra 206 transducer. The initial chamber pressure was atmospheric and the RK315A liquid propellant feeding rate was 4 in/min (0.128 g/s). A series of selected images of the transition to ignition of an elevated pressure test is shown in **Fig. 14**. **Figure 15** reports the pressure and temperature time profiles during an experiment.

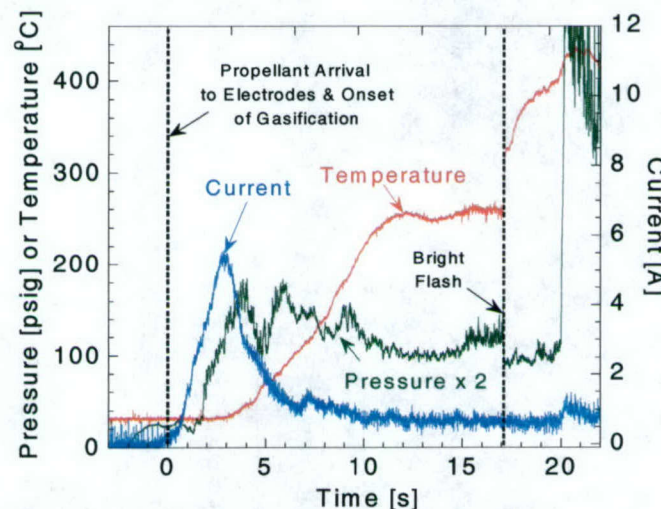


Figure 15. Current, temperature, and pressure profiles illustrating the electrolytic ignition process in a macro-scale igniter.

During the pre-gasification stage, the pressure in the chamber remained atmospheric. The current rapidly increased when the incoming liquid propellant front came in contact with the leading edge of the microfins. Once the liquid propellant began to gasify, the chamber pressure rapidly increased to a pressure of approximately 90 psig, then gradually decayed to around 60 psig. The temperature of the evolved gas was equal to the ambient temperature until the current reached its maximum value, after which the gas temperature began to rise. After 10 seconds, the

product gas temperature attained a constant value of 250°C and remained at this value until a sudden transition to a higher temperature second stage reaction occurred.

The onset of the second stage reaction was evident when the brown cloud inside the chamber transitioned to a clear gas immediately after a bright white flash at around 16 seconds. Subsequent to the second stage reaction, the chamber pressure reached almost 300 psig. The supplied voltage potential was removed around 22 seconds. The liquid propellant feed was stopped at approximately 40 seconds thus terminating the test run. The pressure-time profile became zero when the voltage potential was removed due to a floating ground artifact of the DC circuitry.

The electrolytic reactivity is a maximum shortly after the propellant flow reaches the electrodes as is evident from the maximum in the current profile and from the significant amount of gas that is generated at low temperatures, which results in the pressure rise in the chamber. The electrolysis reactions initiate a thermal reaction producing a temperature rise of the product gases.

Model Development and Analysis of Vortex Flows

In order to obtain understanding of the flame stabilization and spreading processes in small combustion chambers as well as to improve the chamber design, we have been developing three-dimensional codes for treating chemically reacting flows. The formulation is based on the three-dimensional conservation equations of mass, momentum, energy, and species transport for a

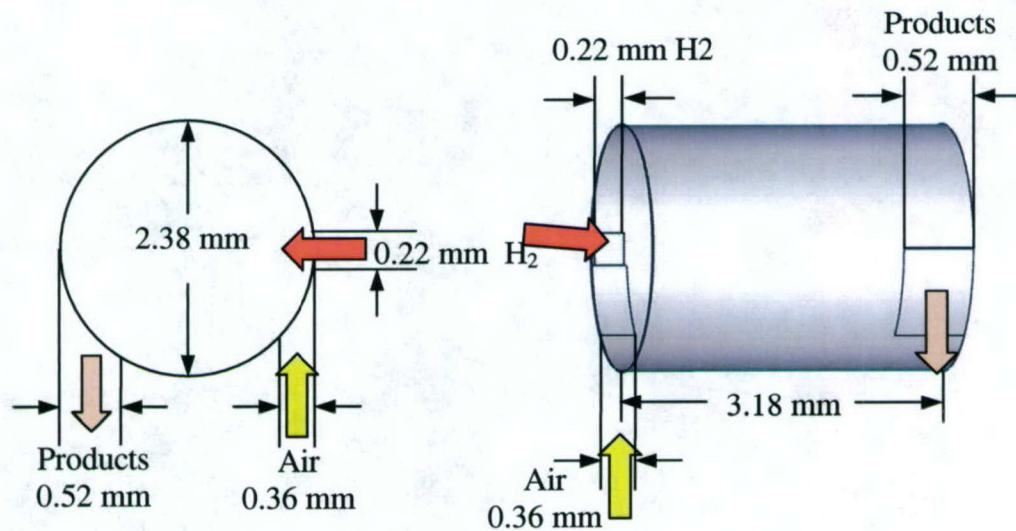


Figure 16. Geometry of the vortex combustor.

multi-component system, and accommodates finite-rate chemical kinetics. Although we have developed the numerical code to implement detailed chemistry and transport, our calculations for hydrogen combustion have been based on a one-step reaction.

Currently, we are solving the governing equations through a density based, finite-volume methodology. The spatial discretization employs a fourth-order and a second-order central difference scheme for convective and viscous terms, respectively. The temporal integration is achieved using a four-step Runge-Kutta algorithm. Further efficiency is obtained by implementing a message passing interface (MPI) parallel computing architecture with a multi-block domain decomposition technique.

The combustor flow has been found to be quite complex in these small volumes. Generally recirculation zones have been found to assist stabilization of the reacting flow. However, the type of recirculation has been found largely dependent on the Reynolds number of the flow, the size of the chamber, the pressure of the chamber, and the manner in which the reactants enter the combustion chamber, as well as the manner in which the products exit the chamber.

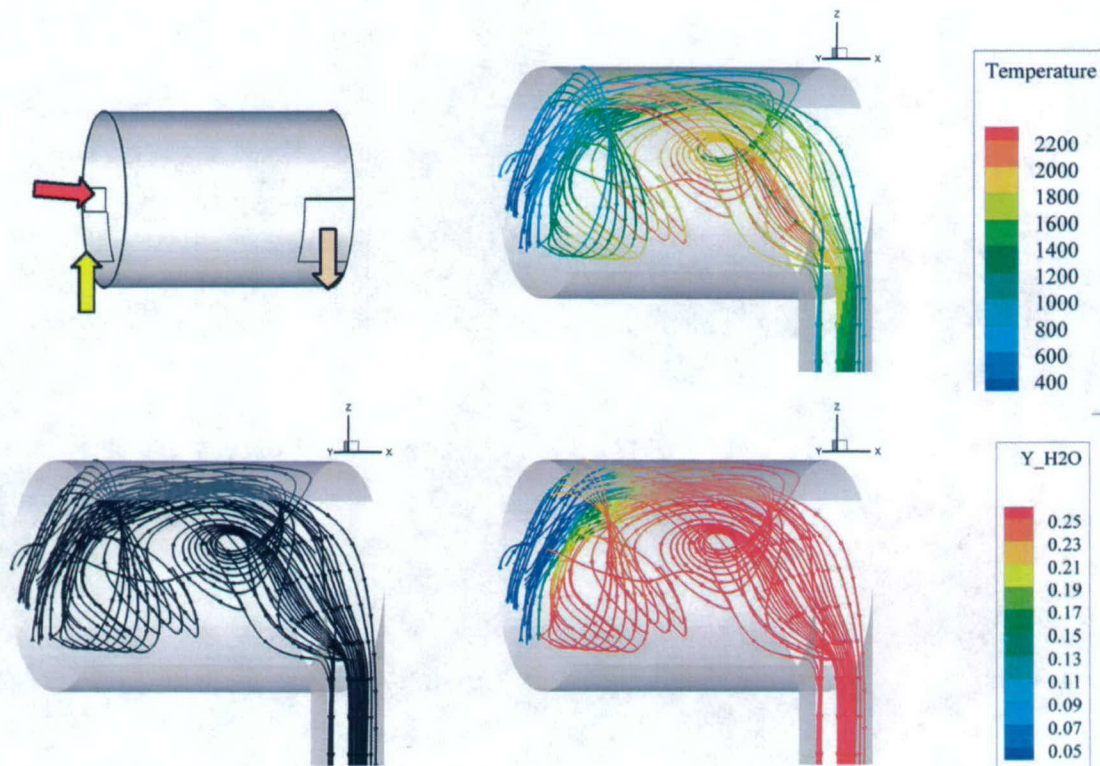


Figure 17. Flow structure in the vortex combustor.

During the past year, the modeling efforts were concentrated on examining the influence of the inlet and exhaust boundary flow geometries on the flame stabilization mechanism. An example of the results is given here for the 2.15 mm diameter combustor operating on a stoichiometric hydrogen air mixture with the flow exiting the combustor tangentially. The geometry of the combustor is shown in **Fig. 16**. The inlet velocity of the air was 100 m/s, the chamber pressure was 1 atm, and the walls were maintained at 800 K. The overall flow field is shown in **Fig. 17** with the temperature and water concentration overlaid on the flow streamlines. The flowfield is essentially made up of three regimes: an outer flow field, which does not recirculate, but rotates about the chamber and accounts for the majority of the mass flow through the chamber, and two minor recirculation paths.

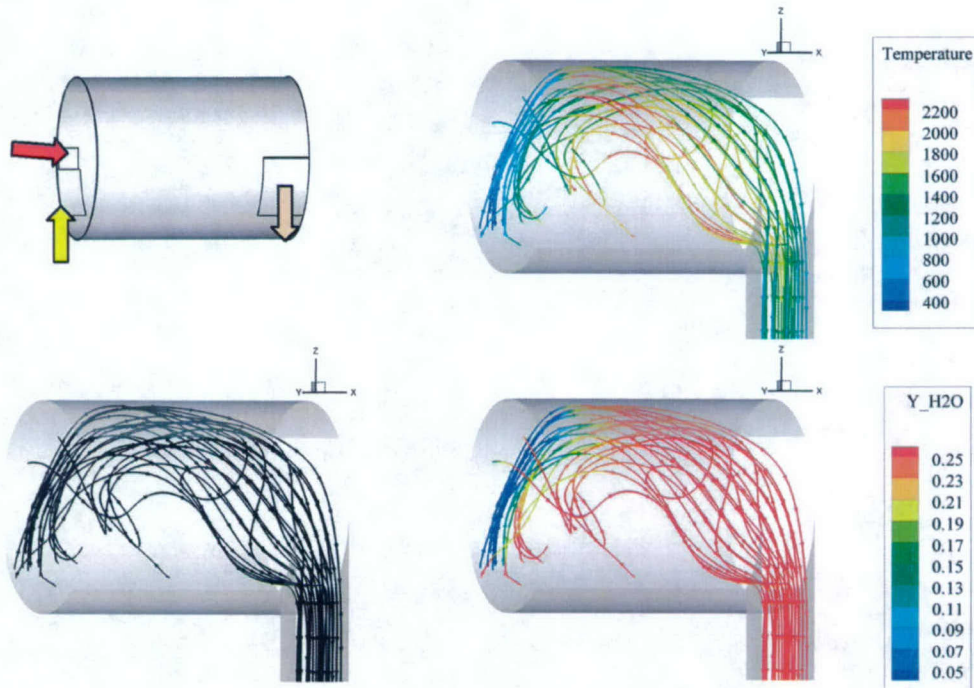


Figure 18. Major flow regime.

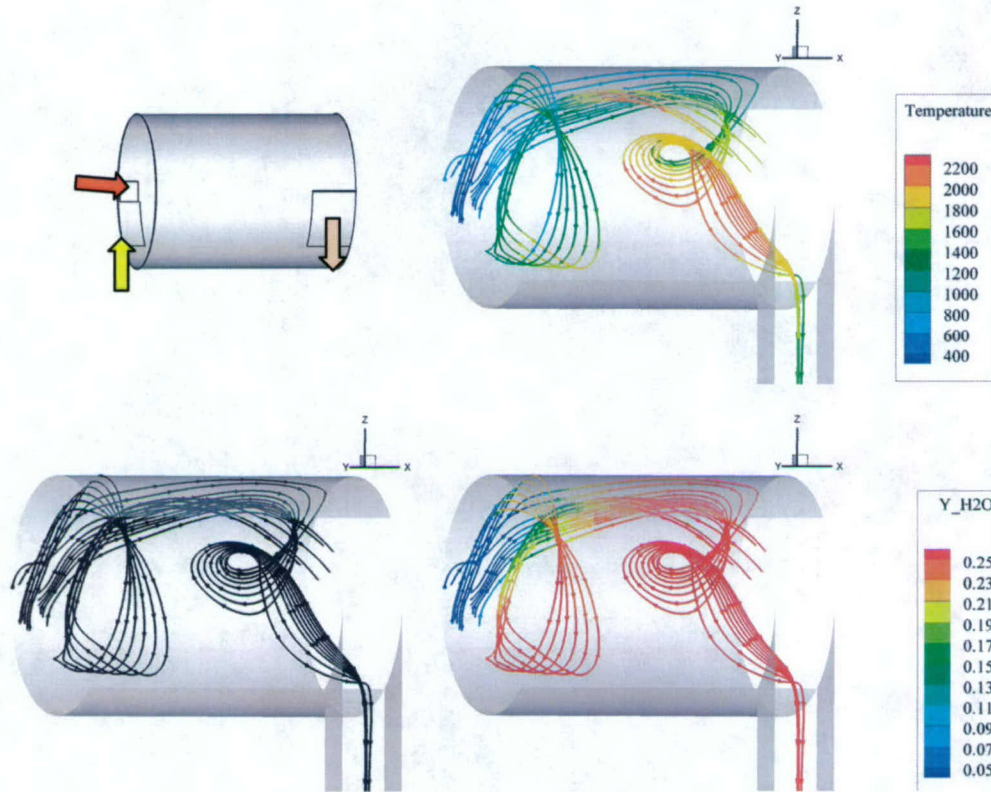


Figure 19. Two minor flow regimes, each with a recirculation zone.

Figure 18 shows the streamlines of the main flow regime and **Figure 19** shows the minor flow streamlines. For the minor streamlines, note that some of the flow recirculates in the front portion of the chamber, whereas another portion of the flow recirculates in the downstream-half of the chamber.

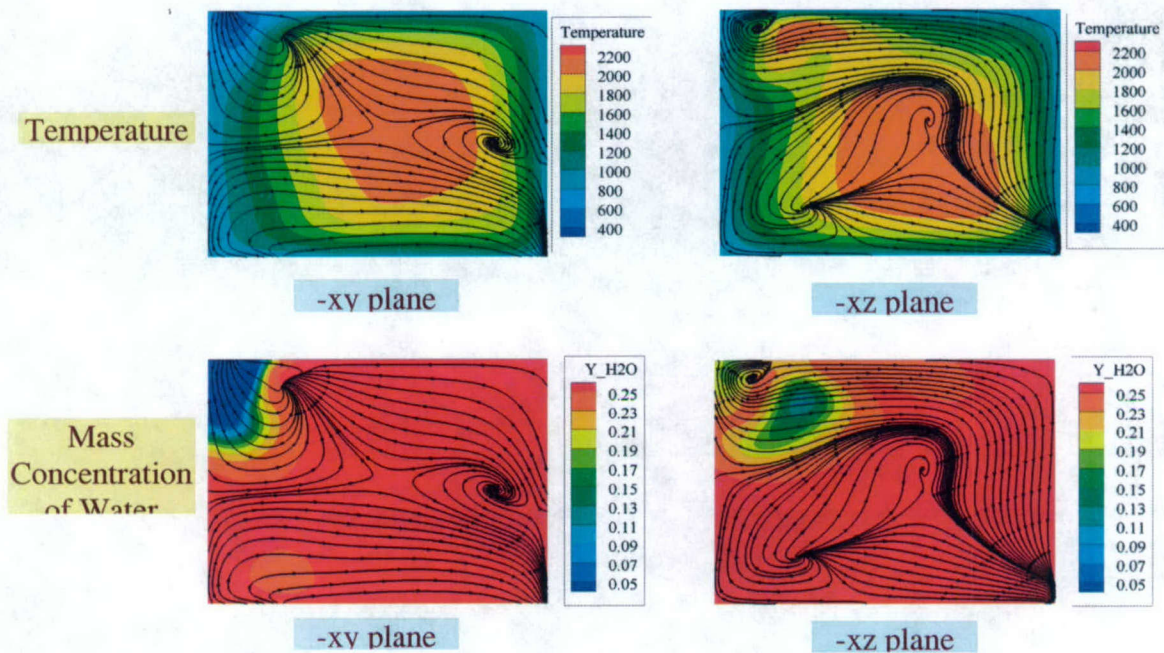


Figure 20. Two dimensional “pseudo” streamlines.

Figure 20 shows the two-dimensional “pseudo” streamlines in the x - y and x - z planes. Note from the temperature contours that the highest temperatures are maintained in the core of the chamber.

SUMMARY

During the past year, small combustors for use in meso- and micro-scale chemical thrusters have been demonstrated to operate directly on liquid monopropellants. Operating pressures in the combustors ranged from 8 to 30 atmospheres and power input levels from 90 to 120 W. Combustor volumes tested were small, typically 108 mm^3 or less. The monopropellants were environmentally “green,” consisting of nitromethane and hydroxyl ammonium nitrate (HAN) water solutions with a dissolvable fuel such as methanol. The liquid propellants were injected tangentially into the combustor along the wall, which when gasified creates a gaseous vortex flow in the combustor that stabilizes a high temperature gas-phase flame with temperatures exceeding 2000 K. In meso- and micro-scale systems, boundary conditions have a significant impact on the overall system performance and reliability, making the couplings between gas-phase flow processes and solid structures much more important than in macro-scale systems.

Here, the thin liquid fuel film provides a large surface area to produce high gasification rates, while at the same time contributing to the overall thermal management of the system by absorbing heat and maintaining the surface temperature close to the boiling/decomposition temperature of the liquid propellant.

Ignition of the monopropellants was accomplished by making use of the electrolytic characteristic of the propellants to reduce power requirements, improve thermal management and eliminate the need for catalyst. Small voltage potentials across electrodes are used to initiate electrochemical reactions, which lead to gasification and high temperature combustion. This ignition system deposits electrical energy directly into chemical energy of the propellant bypassing the need for thermal energy to raise the surface temperature of a catalyst to its ignition temperature. The technique was successfully demonstrated in various-size igniters with HAN based monopropellants. In these igniters, a DC voltage potential was applied across a set of electrodes and then the propellant flow was started. Immediately upon contact of the propellant with the electrodes, gasification was initiated. A meso-scale igniter was tested with 500 μm channels, which can be connected directly to the liquid propellant combustor and will be used to initially ignite the liquid propellant after which the power will be removed.

RECENT PUBLICATIONS AND PRESENTATIONS

- Combustion in Meso-scale Vortex Combustors: Experimental Characterization, M.-H. Wu, R.A. Yetter, and V. Yang, 42nd Aerospace Sciences Meeting & Exhibit, 5-8 January 2004, Reno, Nevada, AIAA 2004-0980.
- Numerical Study on Swirling Flow in a Cylindrical Chamber, Y. Wang, V. Yang, and R.A. Yetter, 42nd Aerospace Sciences Meeting & Exhibit, 5-8 January 2004, Reno, Nevada, AIAA 2004-0981.
- An Integrated Experimental and Numerical Study of Meso-Scale Vortex Combustor Dynamics, Y. Wang, Wu, M., R.A. Yetter, and V. Yang, 43rd Aerospace Sciences Meeting & Exhibit, 10-13 January 2005, Reno, Nevada, AIAA 2005-0941.
- Combustion Issues and Approaches for Chemical Microthrusters, R.A. Yetter, V. Yang, I.A. Aksay, and F.L. Dryer, Invited Paper, 6th International Symposium on Chemical Propulsion, Santiago, Chile, March 2005, **Martin Summerfield Best Paper Award**.

REFERENCES

1. Koeneman, P.B. Bush-Vishniac, I.J., and Wood, K.L., J. MEMS Systems 6, (4) 355 (1997). Nowak, R., "Batteries and Fuel Cells," MEMS Based Microscale Power Generation and Energy Conversion Concepts and Systems, DARPA Workshop, Arlington, VA, February 27-28, 1998.
2. Gad-el-Hak, M., "Microdevices-The Freeman Scholar Lecture," Journal of Fluids Engineering, 121, 5, March 1999.
3. Gad-el-Hak, M. "Challenges in the Understanding of Microscale Phenomena," AIAA 2003-439, 41st Aerospace Sciences Meeting and Exhibit, 6-9 January 2003 Reno, NV.
4. Helvajian, H., ed., Microengineering Aerospace Systems, The Aerospace Press, El Segundo, CA, and AIAA, Reston, VA, 1999.
5. Micci, M.M. and Ketsdever, A.D., eds., Micropropulsion for Small Spacecraft, Progress in Astronautics and Aeronautics, Vol. 187, AIAA, Reston, VA, 2000.
6. Fernandez-Pello, A.C., "Micropower Generation using Combustion: Issues and Approaches," Proc. Comb. Inst. 29, 883-899, 2002.
7. Chigier N. and Gemci, T., "A Review of Micro Propulsion Technology," AIAA 2003-670, 41st Aerospace Sciences Meeting and Exhibit, 6-9 January 2003 Reno, NV.
8. Janson, S.W., "Chemical and Electric Micropropulsion Concepts for Nanosatellites," AIAA 94-2998, 30th AIAA/ASME/SAE/ASEE Joint Propulsion Conference, Indianapolis, June 1994.
9. DeGroot, W.A. and Oleson, S.R., "Chemical Microthruster Options," AIAA 96-2863, 32nd AIAA/ASME/SAE/ASEE Joint Propulsion Conference, Buena Vista, FL, July 1996.
10. Mueller, J., "Thruster Options for Microspacecraft: A Review and Evaluation of Existing Hardware and Emerging Technologies," AIAA 97-3058, 33rd AIAA/ASME/SAE/ASEE Joint Propulsion Conference, Seattle, WA, July 1997.
11. Janson, S.W., Helvajian, H., and Breuer, K., "Micropropulsion Systems for Aircraft and Spacecraft," in Microengineering Aerospace Systems, ed. Helvajian, H., The Aerospace press, El Segundo, CA, 1999.
12. Janson, S.W., Helvajian, H., Hansen, W.W., and Lodmell, J., "Batch-Fabricated CW Microthrusters for Kilogram-Class Spacecraft," AIAA 99-2722, 35th AIAA/ASME/SAE/ASEE Joint Propulsion Conference, 20-24 June 1999, LA.
13. Rodgers, S.L., Carrick, P.G., and Berman, M.R., "Propellants for Microthrusters," in Microengineering Aerospace Systems, ed. Helvajian, H., The Aerospace press, El Segundo, CA, 1999.
14. Ketsdever, A.D. and Mueller, J., "Systems Considerations and Design Options for Microspacecraft Propulsion Systems," AIAA 99-2723, 35th AIAA / ASME / SAE / ASEE Joint Propulsion Conference and Exhibit, 20-24 June 1999 Los Angeles, CA.
15. Ketsdever, A.D., Wadsworth, D.C., Wapner, P.G., Ivanov, M.S., and Markelov, G.N., "Fabrication and Predicted Performance of Conical DeLaval Micronozzles," 35th AIAA/ASME/SAE/ASEE Joint Propulsion Conference, 20-24 June 1999, LA.
16. Ketsdever, A.D., "Microfluidics Research in MEMS Propulsion Systems," AIAA 2003-0783, 41st Aerospace Sciences Meeting & Exhibit, 6-9 January 2003, Reno, NV.
17. Sethu, P. and Mastrangelo, C.H., "Polyethylene Glycol (PEG)-based Actuator for Nozzle-Diffuser Pumps in Plastic Microfluidic Systems," Sensors and Actuators A 104, 283-289, 2003.
18. Rossi, C., Esteve, D., Temple-Boyer, P., and Delannoy, "Realization, Characterization of Micro Pyrotechnic Actuators and FEM Modeling of the Combustion Ignition," Sensors and Actuators A, 70, 141-147, 1998. Rossi, C., Esteve, D., and Mingues, C., "Pyrotechnic Actuator: A New Generation of Si Integrated Actuator," Sensors and Actuators, 74, 211-215, 1999.

19. Klintberg, L., Karlsson, M., Stenmark, L., and Thornell, G., "A Thermally Activated Paraffin-Based Actuator for Gas-flow Control in a Satellite Electrical Propulsion System," *Sensors and Actuators A* 105, 237-246, 2003.
20. Davis, T., XSS-10 Microsatellite Flight Demonstration Program, AFRL Technology Horizons, December 2004, p. 10.
21. Yetter, R.A., Yang, V., Aksay, I. A., and Dryer, F.L., Meso and Micro Scale Propulsion Concepts for Small Spacecraft, AFOSR Final Report, F49620-01-1-0376, December 2004.
22. Yetter, R.A., Yang, V., Wang, Z., Wang, Y., Milius, D., Aksay, I.A., and Dryer, F.L., "Development of Meso and Micro Scale Liquid Propellant Thrusters," AIAA 2003-0676, 41st Aerospace Sciences Meeting & Exhibit, 6-9 January 2003, Reno, NV.
23. Schöyer, H.F.R., Korting, P.A.O.G., Veltmans, W.H.M., Louwers, J., v.d. Heijden, A.E.M., Keizers, H.L.J., and v.d. Berg, R.P., "An Overview of the Development of HNF and HNF-based Propellants," 36th AIAA/ASME/SAE/ASEE AIAA Joint Propulsion Conference & Exhibit, Huntsville, Al., 17-19 July 2000.
24. Anflo, K., Grönland, T.A., and Wingborg, N., "Development and Testing of ADN-Based Monopropellants in Small Rocket Engines," A00-36427, 36th AIAA/ASME/SAE/ASEE AIAA Joint Propulsion Conference & Exhibit, Huntsville, Al., 17-19 July 2000.
25. Jankovsky, R.S., "HAN-Based Monopropellant Assessment for Spacecraft," AIAA 96-2863, 32nd AIAA/ASME/SAE/ASEE Joint Propulsion Conference, Lake Buena, Vista, FL, 1996.
26. E.J. Wucherer and S. Chrisofferson "Assessment of High Performance HAN-Monopropellants," 36th AIAA / ASME / SAE / ASEE Joint Propulsion Conference 16-19 July 2000, AIAA A00-36948.
27. Stanchi, S., Dunn-Rankin, D., Sirignano, W.A., "Combustor Miniaturization with Liquid Fuel Filming," AIAA 2003-1163, 41st Aerospace Sciences Meeting and Exhibit, 6-9 January 2003 Reno, NV.
28. N. Klein, "The Molecular Structure of the HAN-Based Liquid Propellants," AD-A226 415.
29. Risha, G.A., Yetter, R.A. and Yang, V., Electrolytic Ignition of Advanced HAN-Based Liquid Propellants for Space Propulsion Systems, Final Report, Air Force Research Laboratory, Edwards Air Force Base, Contract No. F04700-03-M-5061, May 2005.